ACS APPLIED MATERIALS & INTERFACES

Research Article

www.acsami.org

Magnetically Aligned Nanodomains: Application in High-Performance Ion Conductive Membranes

Mohammad Mahdi Hasani-Sadrabadi,*[,†,‡,§,∥] Fatemeh Sadat Majedi,[∥] Géraldine Coullerez,*[,§] Erfan Dashtimoghadam,[⊥] Jules John VanDersarl,[‡] Arnaud Bertsch,[‡] Homayoun Moaddel,[▲] Karl I. Jacob,*[,†] and Philippe Renaud*[,‡]

[†]School of Materials Science and Engineering and G. W. Woodruff School of Mechanical Engineering, Georgia Institute of Technology, Atlanta, Georgia 30332-0245, United States

[‡]Laboratory of Microsystemes (LMIS4), Institute of Microengineering, [§]Laboratory of Powder Technology, Institute of Materials, École Polytechnique Fédérale de Lausanne (EPFL), Station 17, CH-1015 Lausanne, Switzerland

[∥]Center of Excellence in Biomaterials, Department of Biomedical Engineering, [⊥]Department of Polymer Engineering and Color Technology, Amirkabir University of Technology, Tehran 15875-4413, Iran

[▲]Hydrogen & Fuel Cell, Inc., Arcadia, California 91006, United States

ABSTRACT: Polyelectrolyte-coated magnetic nanoparticles were prepared by decorating the surface of superparamagnetic iron oxide nanoparticles (SPIONs) with crosslinked chitosan oligopolysaccharide (CS). These positively charged particles (CS-SPIONs) were then added to a negatively charged polymer (Nafion), and cast into membranes under an applied magnetic field. TEM and SAXS measurements confirmed this process created aligned, cylindrical nanodomains in the membranes. This was also indirectly confirmed by proton conductivity values. The strong electrostatic interaction between chitosan and Nafion prevented oxygen permeability and water evaporation at elevated temperatures through the proton conductive channels. The resultant proton exchange membranes showed lower conduction dependency to relative humidity, which is highly desirable for hydrogen fuel cells. The fuel cell performance tests were performed on the designed polyelectrolyte membrane by hydrogen−oxygen single cells at elevated temperature (120 °C) and low relative humidity.

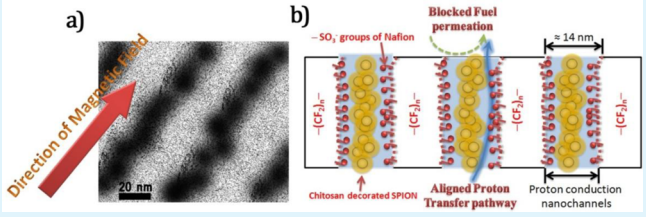

KEYWORDS: *polymer-decorating nanoparticles, SPION, aligned nanodomains, nanocomposite membranes, proton conductivity, fuel cell*

1. INTRODUCTION

Fuel cell technologies are being rapidly developed as promising alternative power sources because of their environmental advantages and high efficiencies. Fuel cells provide several advantages over other energy conversion devices, including modularity, eco-friendliness, multi-fuel compatibility and low maintenance costs.[1] During the past years, several types of fuel cells have been developed,[2] with proton exchange membrane fuel cells (PEMFCs) among the most promising for transportation applications, owing to their high energy density at medium operating temperatures. The proton exchange membrane (PEM) is a central component, acting as the fuel barrier and providing proton conduction.[1] Perfluorosulfonate ionomers, developed by DuPont known as Nafion, are currently the most popular commercial polyelectrolyte membrane for PEMFC applications, which is on account of their high thermochemical stability and good proton conductivity.[3]

A recent morphological study of Nafion confirms the presence of parallel hydrophilic channels that are randomly distributed laterally.[4,5] These channels are key to PEM transport properties,[5] and processing techniques, such as solution casting,[6] melt extrusion, thermal annealing, electrospinning,[7−9] and uniaxial extension,[10] have been used thus far to adjust film morphology, and tune transport properties. However, these methods can induce anisotropic in-plane proton conductivity to the PEM, which is not beneficial in PEMFC applications.

Recent research into improving the transport properties of PEMs has shown increasing proton conductivity in the membrane normal direction is the most effective technique.[11−13] A technical key is thus developing polyelectrolyte films with improved unidirectional proton conduction through the membranes.[12,13] With this objective, some researchers have focused on enhanced transport properties in PEMs with oriented ionomeric microstructures.[11−13]

Induced nanodomain alignment normal to the surface of membrane by the application of electric fields[14−17] or flow fields[18] has already been demonstrated. However, as connection of micro-/nano- domains is difficult to obtain across a

Received: December 30, 2013
Accepted: April 30, 2014
Published: April 30, 2014

macroscopic length scale, the anisotropic proton conduction in these films was not very high.[19]

The directional ordering of both functional microparticles and nanoparticles in a matrix has been successfully demonstrated using an electrical field.[14,15] However, this ordering can only be achieved while particles and the matrix show sufficient dielectric disparity. An alternative method to induce alignment is through the application of a magnetic field.[20,21] With this approach, sufficient saturation magnetization of nanoparticles is required to respond to the applied magnetic field. Shaw and coworkers used this concept to orient sulfonated crosslinked polystyrene coated γ-Fe_2O_3 core-shell particles (230-340 nm) in sulfonated poly(ether ketone ketone) (SPEKK). However, these ordered composites have lower proton conduction than pure SPEKK, which has been attributed to low ion exchange capacity (IEC) of the particles.[16,22] Hasanabadi et al. recently reported the design of anisotropic polyelectrolyte membranes composed of 100 nm γ-Fe_2O_3 nanoparticles in a sulfonated poly(ether sulfone) matrix, and investigated the effect of alignment on the primary properties of PEM for methanol fuel cell applications.[23] It has been reported smaller nanoparticles (~20 nm) in the range of conductive microdomains could less affect the microstructure of the polyelectrolyte matrices or even incorporate into the ionomeric nanochannels and improve the conductivity.[24] Moreover, it has been shown nanohybrid polyelectrolytes comprising polyelectrolyte complexation at the interface of nanoparticles with ionomeric matrices provide improved transport properties (proton conductivity and fuel permeability).[25,26] To exploit such favorable features simultaneously, here we demonstrate surface decoration of ultrasmall SPIONs with polycationic chitosan oligosaccharide chains. This allows SPION nanoparticles to maintain their small size, while enabling them to interact with the anionic moieties of Nafion.

2. EXPERIMENTAL SECTION

2.1. Materials and Methods. Superparamagnetic iron oxide nanoparticles (SPIONs) were synthesized via alkaline co-precipitation of ferric and ferrous chlorides in aqueous media. The synthesis procedure has been reported in details elsewhere.[27]

2.2. Preparation of Magnetic Chitosan Nanoparticles. Decoration of SPIONs with chitosan biopolymer chains was performed based on an established suspension cross-linking technique.[28] Briefly, 2 w/v% of chitosan oligosaccharide lactate (Aldrich; M_n= 5 kDa) solution was prepared containing SPIONs (10 mg.ml^{-1}). This solution was added dropwise to 60:1 paraffin and span-80 (a nonionic surfactant, $C_{24}H_{44}O_6$) mixture under ultrasonication. A glutaraldehyde solution was then added to the dispersion as a cross linking agent, and the solution was stirred for 6 h. Afterwards, decorated nanoparticles were separated by a permanent magnet, centrifugation, washed with ethanol and distilled water, and then dried at 60 °C before characterization.

2.3. Membrane Preparation. Nanocomposite PEMs, comprising 2.0 wt % of nanoparticles, were fabricated using the solution casting technique. Chitosan decorated SPIONs (CS-SPIONs) were dispersed in deionized water, ultrasonicated for 30 min, subsequently mixed with Nafion dispersion at 25 °C, and stirred for 2.5 h. Afterward, the resultant suspension was cast on a glass Petri-dish and incubated between two poles of a low-impedance magnet with the ability of generating a uniform magnetic field. Then, a 0.1 T magnetic field was applied to align the SPIONs, with a dwell time of 12 h to ensure the evaporation of solvents. Nanocomposite membranes were also prepared with the same procedure, but in the absence of magnetic field incubation step. Pristine Nafion was also cast under magnetic field as the reference sample.

2.4. Fabrication of Membrane Electrode Assembly (MEA). The MEAs were fabricated with the catalyst painting method. The details of MEA preparation procedure have been reported before.[9,29,30]

2.5. Characterization Methods. Chitosan-coated SPIONs as well as the corresponding nanocomposite with Nafion were characterized through transmission electron microscopy method (TEM; CM200-FEG-Philips). In the case of CS-SPIONs, dilute suspensions of sample were deposited onto the carbon films supported with Cu grids. The particles size and morphology were investigated by diffraction (amplitude) contrast, and for crystalline materials, by phase contrast (high resolution) imaging. The apparatus was operating at an accelerating voltage of 200 kV.

To obtain a TEM image from a cross section of the membrane, a thin gold layer was sputtered on the samples. The membranes were then embedded into an epoxy resin and cured at 60 °C for 24 h. Ultrathin TEM sections with thicknesses of ~70 nm were provided by microtomy (Leica Ultracut) using a diamond knife.[31]

The size of nanoparticles was characterized via dynamic light scattering (DLS) by means of Zetasizer 3000HS (Malvern Instruments Ltd.) at 173° at pH 7.4 and 25 °C. The same device was also employed to measure Zeta potential of nanoparticles at different pH and 25 °C. Iron content in nanoparticles was measured through inductively coupled plasma−optical emission spectroscopy (PerkinElmer, Optima ICP-OES) after digestion of nanoparticles in HCl.

The magnetic characteristics of nanoparticles were determined via a vibrating sample magnetometer (VSM, ADE 4HF) at the ambient temperature.

Before swelling measurements, membranes were fully dried in oven, weighed, and then soaked in deionized water and reweighed at different time intervals. This process was repeated until no further increase in weight was observed. Water uptake was calculated according to eq 1

$$\text{water uptake } (\%) = 100 \times \left(\frac{M_{\text{wet}} - M_{\text{dry}}}{M_{\text{dry}}} \right) \tag{1}$$

where M_{wet} and M_{dry} are, respectively, the weights of membrane samples in wet and dry states.

The molar ratio of water molecules to the sulfonate groups, indicated as lambda (λ), was calculated according to eq 2

$$\lambda = \frac{\text{WU}}{\text{IEC} \times M_{\text{water}}} \tag{2}$$

where IEC, WU, and M_{water} are the ion exchange capacity, water uptake, and water molecular weight (18 g mol^{-1}), respectively. In fact, λ indicates number of water molecules which can be bound onto the ionic groups on polyelectrolyte chains. Hydration of polyelectrolytes and proton conductivity are commonly explained with λ.

The designed polyelectrolyte membranes were also studied by small angle X-ray scattering (SAXS) technique. SAXS experiments were performed by means of a diffractometer with Cu K source and Kratky SAXS equipment. Hydrated samples were placed in a sample holder at 25°C. The chamber was kept under vacuum. The scattering intensity is plotted versus the scattering vector, q, defined as $q = (4\pi/\lambda) \sin \theta$, where 2θ and λ are the scattering angle and X-ray wavelength.

Fabricated membranes were characterized for their bulk proton conductivity using a BT-112 conductivity cell (BekkTech LLC). Conductivity of membranes was calculated based on eq 3:

$$\sigma = \frac{L}{RA} \tag{3}$$

where L, R, and A, respectively, refer to membrane thickness, resistance, and cross-sectional area. In this study, conductivity of membranes was measured at various relative humidity (RH 20−100%). To study the effect of temperature on conductivity, temperature-sweep proton conduction measurements were performed from 25 to 120 °C. The conductivity cell was incubated in a chamber at a predetermined RH for 3 h prior to measurements.

The oxygen permeability through membranes (P) was determined based on the constant pressure/variable volume method at 25 °C via a laboratory made test cell using the following equation: $P = Ql/[A(p_1 - p_2)]$, where Q, l, A, p_1, and p_2 are, respectively, the flow rate of the permeate molecules, membrane thickness, effective membrane area, absolute pressures of feed side and permeate side. The permeability coefficient is expressed in Barrer units ($\times 10^{10}$ $cm_{(STP)}{}^3$ cm cm^{-2} s^{-1} cm Hg^{-1}).

PEMFC tests on designed membranes were carried out by a laboratory made single cell. The details of the fuel cell performance tests have been reported elsewhere.[32]

3. RESULTS AND DISCUSSION

As shown in Figure 1a, surface decoration of SPIONs with chitosan can be achieved with a relatively small change in the diameter of SPIONs. The relatively small increase in diameter, from 13 to 18.2 nm, is attributed to decoration of nanoparticles with the low molecular weight polysaccharide chains. TEM images of CS-SPIONs, Figure 1c, also confirmed the creation of a thin chitosan shell (3.5 ± 1 nm) on the SPION surface, Figure 1b.

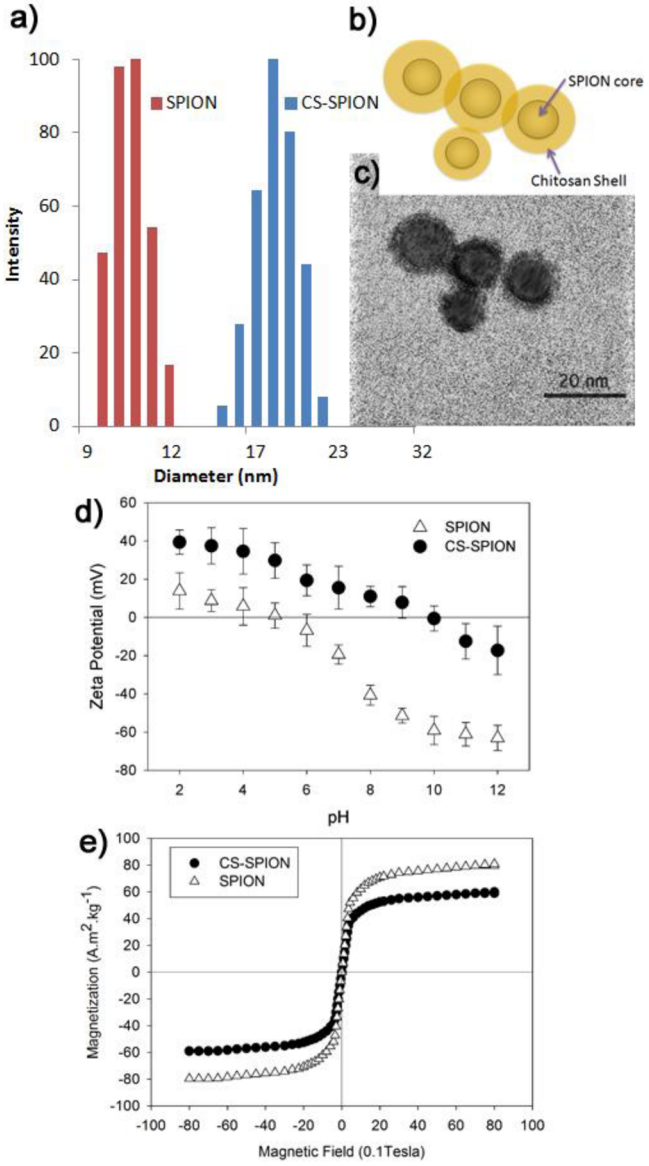

Figure 1. Representative DLS graphs of pristine and chitosan coated SPIONs (CS-SPIONs) (a). In panels b and c, a schematic and TEM images in which the SPIONs have been decorated with a chitosan layer, are shown, respectively. ζ potential values as a function of pH are displayed in panel d. Magnetic hysteresis for the CS-SPIONs, as well as pristine SPIONs (e).

The surface charge of the bare and coated nanoparticles at different pHs is shown in Figure 1d. The pristine SPIONs have a slightly positive surface charge below pH 5. The ζ potential of CS-SPIONs is larger than SPIONs, and reached 39 mV in comparison with 14 mV for pristine SPION at a pH of 2. This dramatic difference is associated with the presence of protonated amine groups on the chitosan chains. This level of surface charge confirms the successful covering of the SPION surface by $-NH_3^+$ terminated chitosan chains. Around pH 10 the surface potential of CS-SPIONs decreases to almost zero mV, indicating the loss of protonated groups. Moreover, CS-SPIONs show good particle stability, and the precipitation of CS-SPIONs does not occur at any pH, due to the steric repulsion of the chitosan chains. As reported previously, chitosan oligosaccharide and its magnetic particle conjugate are water-soluble and have favorable interactions with the surrounding medium.[33] This high level of surface charge is essential to making a strong electrostatic interaction with Nafion during device operation.

The hysteresis loop of pristine and chitosan coated SPIONs at room temperature is shown in Figure 1e. The absence of remanence and coercivity confirms the superparamagnetic properties of modified SPIONs. As shown, the magnetic saturation was about 80 A m^2 kg^{-1} for bare magnetite and about 60 emu g^{-1} for CS-SPIONs, which implies a magnetite content of 75 wt % in the coated nanoparticles.

Nafion-based membranes in this study were prepared via the solvent casting method under an applied magnetic field. It has been demonstrated that phase separation of Nafion occurs more efficiently in aqueous solutions compared to organic solvents.[6] Fortunately, CS-SPIONs are fully dispersible in water, which is highly desirable for thorough mixing with the Nafion solution. Moreover, as previously demonstrated[25,34] electrostatic interactions among amine groups of chitosan layer and the sulfonate groups on Nafion chains can control ionic phase separation in Nafion.

A cross sectional HRTEM image of the aligned nanocomposite displayed in Figure 2c clearly confirms a chain-like assembly of the CS-SPIONs because of the magnetic field. The CS-SPIONs are aligned in the direction of induced magnetic field and form a worm-like geometry with a diameter of 19 ± 2 nm. A diagram of the proposed microstructure for nonaligned/aligned are shown in Figure 2b and d.

To verify formation of aligned nanochannels, the membranes were characterized using small-angle X-ray scattering (SAXS), Figure 2e. Nafion shows a scattering peak at 0.55 nm^{-1}, which is an indication of self-assembled nanostructures with a d-spacing of 11.42 nm. In the case of magnetically aligned Nafion/CS-SPION this peak moves to around q= 0.45 nm^{-1}, which indicates the expansion of the nanochannels to 13.96 nm. The higher intensity peak confirms higher levels of phase separation by presence of CS-SPION due to the additional electrostatic interactions, as well as the applied magnetic field. Interestingly, the clear appearance of a second-order peak at $\sqrt{3}q^*$ suggests a hexagonally packed tube-structure of nanodomains.[35]

To test the strength of the electrostatic interactions between the functionalized nanoparticles and the matrix, SAXS experi-

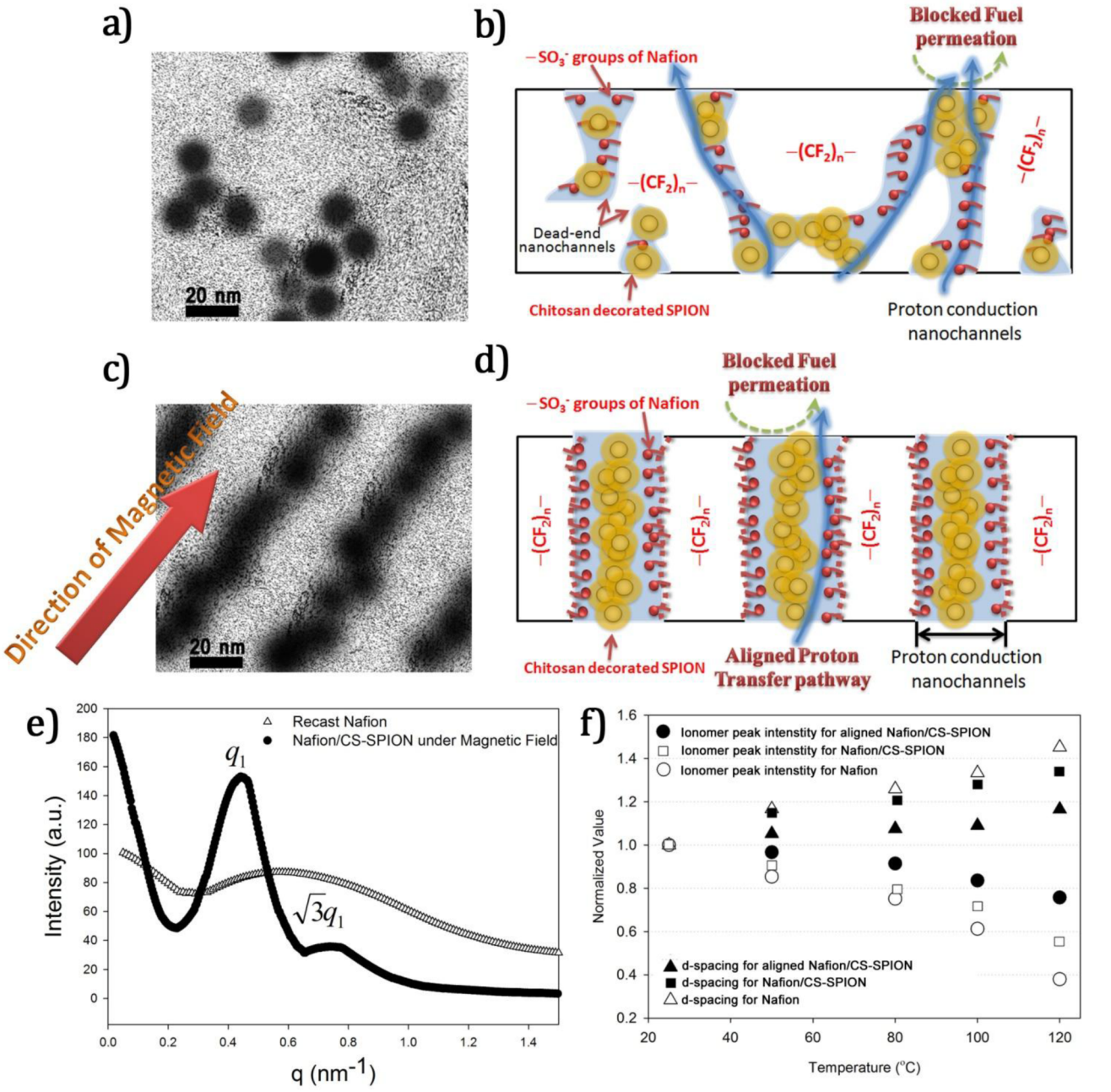

Figure 2. High resolution transmission electron microscopy (HRTEM) shows dispersion of chitosan coated magnetic nanoparticles (CS-SPION NPs) inside Nafion matrix without external magnetic field (a). as well as chain-like assembly of CS-SPION NPs in the presence of applied magnetic field (c). Schematic representation of the proposed microstructure for randomly dispersed nanoparticles (b) and unidirectional orientation of ion-conduction nanochannels (d). Small angle X-ray scattering patterns (intensity vs. scattering vector, q) for aligned nanocomposite membranes compared to the corresponding pristine Nafion membrane. The ionomer peak position at maximum intensity is used to calculate the d-spacing (e). Temperature dependency (25−120 °C) of ionomer peak intensity and *d*-spacing for aligned/non-aligned nanocomposite membranes and pristine Nafion, normalized to their values at 25°C (f).

ments were also performed at different temperatures in the range of 25 to 120 °C. Figure 2f shows experimental results normalized to the values at 25 °C.

As summarized in Figure 2f, in the presence of CS-SPION nanoparticles inside the Nafion matrix the structural stability of membranes was found to be increased with temperature. In other words, less fluctuation of the *d*-spacing value for Nafion matrix loaded with coated SPION nanoparticles implies the effective interfacial role of chitosan on the microstructural as well as transport properties of the designed Nanohybrid polyelectrolytes. For aligned nanocomposite membranes, the ionomer peak intensity has a low dependency on temperature, which is an indication of the stabilizing of the microstructure obtained when using the magnetically aligned Nafion/chitosan-coated SPION. The nanochannels diameters stabilize over a wide temperature range, swelling less than 17% over the entire interested temperature range. For the pristine Nafion membrane, intensity of the first-order scattering peak decreased significantly with increasing temperature. Moreover, the *d*-spacing also increased by about 45% from 11.60 to 16.9 nm.

dx.doi.org/10.1021/am406042w | ACS Appl. Mater. Interfaces 2014, 6, 7099−7107

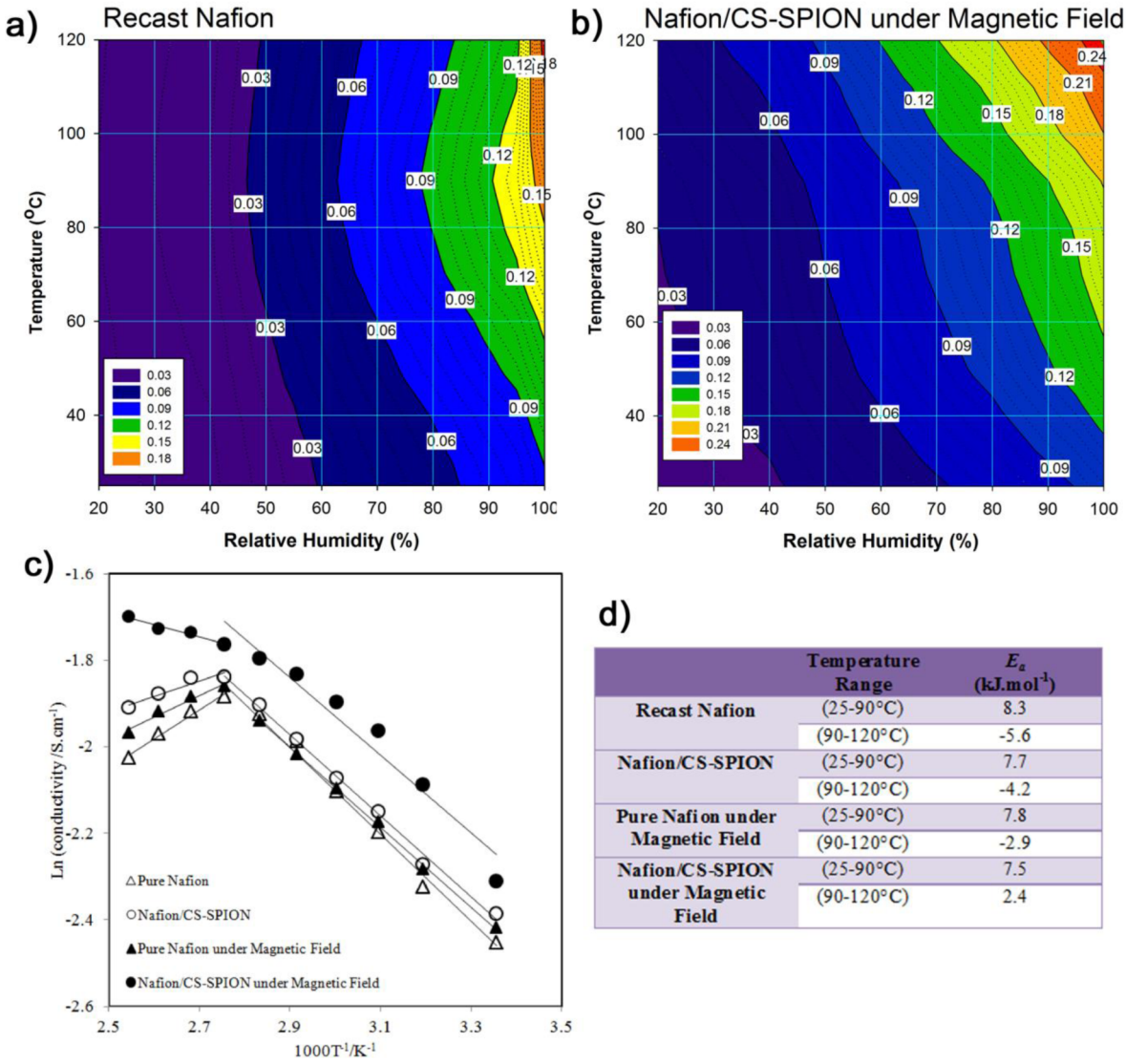

	Temperature Range	E_a (kJ.mol^{-1})
Recast Nafion	(25-90°C)	8.3
	(90-120°C)	-5.6
Nafion/CS-SPION	(25-90°C)	7.7
	(90-120°C)	-4.2
Pure Nafion under Magnetic Field	(25-90°C)	7.8
	(90-120°C)	-2.9
Nafion/CS-SPION under Magnetic Field	(25-90°C)	7.5
	(90-120°C)	2.4

Figure 3. Counter plots of proton conductivity at various temperatures (25−120 °C) and different relative humidity (RH = 20−100%) of (a) recast Nafion and (b) Nafion/CS-SPION membranes, which are formed under magnetic field. The proton conductivity values are shown on interval lines in the dimension of [S cm^{-1}]. (c) Arrhenius plot of proton conductivity. (d) Activation energy of proton conductivity below and above 90 °C.

These SAXS experiments were carried out at fully humidified condition and the results indicate that pure recast Nafion channels start to swell.

However, this is a result of the breakdown in the Nafion microstructure, which leads to the reduction in membrane conductivity at elevated temperature. For the aligned nanocomposite membranes, high-temperature conductivity can be achieved because of the presence of strong electrostatic interactions between chitosan at the surface of SPIONs and the Nafion matrix.

In membranes with nanochannels aligned normal to the surface, the gas permeability increases due to the reduction in membrane tortuosity. The oxygen permeability of recast Nafion membranes is 2.88 barrers, increases to 3.052 barrers for recast Nafion under magnetic field, as evaluated using the constant pressure/variable volume method at 25°C. However, strong interfacial interactions and reduced free volume through CS-SPIONs membranes can actually decrease the permeability to as low as 1.01 barrers for 2 wt % CS-SPIONs filled Nafion without applied magnetic field, and to 1.24 barrers for magnetically aligned CS-SPION filled nanocomposite membranes. This value is more than two fold less than pristine Nafion, an important advancement, as low as possible permeability of fuels is highly desirable in fuel cell applications.[36]

The anisotropic assembly of continuous nanodomains is confirmed by the unidirectional conductivity of the membrane.[18,35] Figure 3c shows that the conductivity of all studied membranes (below 90°C) is enhanced with increasing temperature, which suggests a thermally activated process. CS-SPION filled membranes with induced alignment provide higher proton conduction in all temperature ranges. Increased conduction is likely due to the creation of well-aligned nanochannels which are ion-rich regions for unidirectional proton conduction.

Room temperature conductivity of recast Nafion, recast Nafion under magnetic field, and Nafion/CS-SPION without magnetic field were found to be 0.86 ± 0.04, 0.89 ± 0.06, and 0.92 ± 0.04 S cm^{-1}, respectively. These obtained conductivity values are very close. However, magnetically aligned Nafion/

dx.doi.org/10.1021/am406042w | ACS Appl. Mater. Interfaces 2014, 6, 7099−7107

Table 1. State of Water in Pristine Nafion and Nafion/CS-SPION Membranes with and without Applied Magnetic Fields

	thickness (μm)[a]	water uptake (%)	IEC (mequiv g^{-1})[b]	λ[c]	proportion of bound water (%)	water-retention (%)
recast Nafion	60 ± 5	32 ± 2	0.89	20	42	11
Nafion/CS-SPION	64 ± 7	39 ± 3	0.94	23.0	70	18
pure Nafion under magnetic field	67 ± 3	23 ± 5	0.86	14.9	58	14
Nafion/CS-SPION under magnetic field	65 ± 5	26 ± 4	0.92	15.7	96	21

[a]Membrane thicknesses are calculated based on at least 5 measurements from different sites of membrane. [b]IEC: ion exchange capacity. [c]Lambda (λ) is the ratio of mole number of water molecules to the fixed-charged ionic groups.

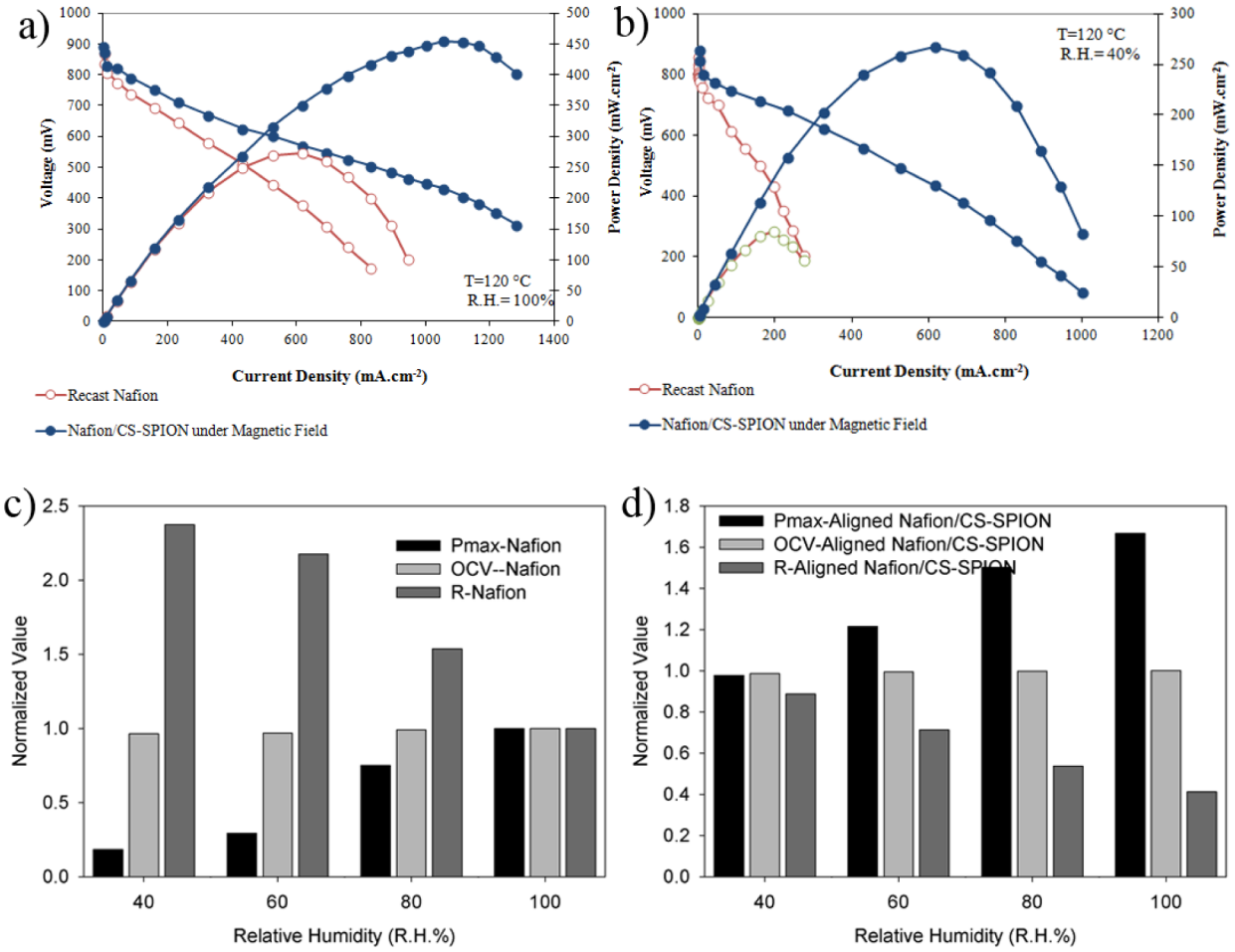

Figure 4. Polarization curves of hydrogen−oxygen single cells consisting of a Nafion nanocomposite with 2.0 wt % of CS-SPION at aligned state as well as recast Nafion, at 40% RH (a) and 100% RH (b) at 120°C. Maximum power density output (P_{max}, in mW cm^{-2}), open circuit voltage (OCV, in mV) and ohmic resistance (R in Ω cm^{-2}) are plotted as a function of relative humidity (40, 60, 80, and 100 RH %) for recast Nafion (c) and aligned Nafion/CS-SPIONs (d); the values calculated from polarization curves and illustrated in normalized form, by calculating the ratio of original values to that of for recast Nafion as a reference at T = 120°C and fully hydrated condition.

CS-SPION membranes showed a higher conductivity of 0.99 ± 0.05 S.cm^{-1} at 25 °C.

Above 90°C, conductivity of the pristine Nafion (with-/out magnetic field) and Nafion/CS-SPION drops (negative conductivity−temperature dependency). This observation in attributed to the water evaporation, which not happened in the case of magnetically aligned Nafion/CS-SPION membranes. In the latter case, conductivity increased to 120°C.

The correlation of conductivity and temperature could be expressed with the Arrhenius equation, $\ln(\sigma) = \ln(\sigma_0) - (E_a/RT)$, where σ, σ_0, E_a, R, and T are, respectively, the proton conductivity (S cm^{-1}), a pre-exponential factor, the activation energy of proton conductivity (kJ mol^{-1}), the universal gas constant (8.31 J·mol^{-1} K^{-1}), and the absolute temperature (K).[24] The activation energies of proton conduction for the neat and nanocomposite membranes have been summarized in Figure 3d. In the case of membranes with ordered spatial arrangement of nanoparticles, the sulfonated groups of Nafion are self-assembled around the ultrasmall aminated nanoparticles to minimize the interfacial energy. Such acid−base interactions makes ion rich sites for easier proton hopping (lower E_a). Hence, membranes with field-induced structure display lower activation energy as compared to pristine and non-ordered membranes.

Because of the highly hydrophilic nature of chitosan, the presence of 2 wt % of CS-SPIONs increases water uptake and ion exchange capacity (IEC) values slightly, as shown in Table 1.

However, the induced alignment of nanochannels using a magnetic field reduces these values because of the confinement and shrinkage of nanochannels. Both of these phenomena converge in magnetic field aligned Nafion/CS-SPIONs membranes, leading to acceptable water adsorption and IEC properties. Differential scanning colorimetric (DSC) studies were also used for characterizing the state of water in Nafion's microstructure.[37] As displayed in Table 1, the portion of bound water to the total water in the membrane was increased to 96%, compared to only 42% for pristine recast Nafion membranes. Since bound water stays in the membrane at elevated temperatures, membrane conductivity can be expected to improve at these temperatures.[32]

Single cell performance of fabricated nanocomposite membranes was performed using humidified (40% and 100% R.H.) hydrogen and oxygen gases at 120 °C. As displayed in Figure 4, by aligning CS-SPIONs in a Nafion matrix, the maximum power density (P_{max}) at 100% R.H. was improved significantly from 273 to 455 mW cm^{-2}. The open circuit potentials (OCVs) were the same for each membrane at 100% RH, at about 890 mV. However, at low humidity (40% RH), the OCV value increased, in the presence of CS-SPION, from 858 to 879 mV. The P_{max} provided by the aligned nanocomposite membranes was observed to be as high as 267 $mW.cm^{-2}$ whereas the highest power density output of the reference Nafion membrane was only 50 mW cm^{-2} at 120 °C and 40% RH.

Furthermore, the water-retention ability of the membranes was tested after being dried at 100 °C for 4 h in a vacuum oven, and were exposed to 40% RH.[38] As shown in Table 1, the combination of magnetic field aligned surface decorated nanoparticles improves the water retaining ability of the membranes, which is highly desirable for low-humidity conditions.

The presence of high levels of bound water results in higher conductivity at lower relative humidity and higher temperatures. The counter plots of proton conductivity [S cm^{-1}] as a function of RH and temperature are shown in Figure 3a and b for recast Nafion (Figure 3a) and for magnetic field aligned Nafion/CS-SPIONs (Figure 3b). Aligned nanocomposite membranes have higher conductivity and lower humidity dependency. The humidity dependency is evaluated based on a logarithmic curve fitting at different temperatures to the following formula: $\sigma=\sigma_s.(R.H.)^a$, where σ_s is the proton conductivity at full hydration. The average value of correlation factor (a) is about 2.41 and 1.37 for recast Nafion and aligned Nafion/CS-SPION, respectively. The a values for recast Nafion under magnetic field and for CS-SPION filled Nafion without the applied field (data not shown) are about 2.13 and 1.82, respectively, which is in agreement with water-retention results.[39] These results confirmed that coupling of magnetically induced alignment with electrostatic interaction can have a synergistic effect on proton conductivity at elevated temperatures and low humidity, which was further confirmed by electrochemical performance testing.

Accordingly, it was found that modified Nafion nanocomposite membranes were able to supply a power output over five times than unmodified Nafion at 120 °C and 40% RH. The enhanced electrochemical performance was mostly attributed to the relatively slow voltage drop in the ohmic polarization region, which we further evaluated by kinetic studies.

Kinetic parameters are derived based on curve fitting on potential versus current density data in the following equation, $E= E_0 - b \log i - R_{ohm} i$. where E and i are the measured cell potential and current, b is the Tafel slope, and R_{ohm} accounts for the linear variation of overpotential with current density, primarily due to the ohmic resistance.[40,41] Interestingly, the ohmic resistance (R_{ohm}), as an indicator of the linear variations of the overpotential with current density of the cell, during operation reduced significantly from 0.80 to 0.33 Ω cm^{-2} at 100% RH and from 1.90 to 0.71 Ω cm^{-2} at 40% R.H. This is due to the inclusion of the CS-SPIONs, which is confirmed by the high proton conductance through the ion exchange membrane at elevated temperatures and low humidity conditions. Humidity dependency of P_{max}, OCV, and ohmic resistance (R_{ohm}) are also shown in Figure 4 for recast Nafion (Figure 4c) and aligned Nafion/CS-SPIONs (Figure 4d). The values are calculated from polarization curves and illustrated in normalized form, by calculating the ratio to that of fully hydrated recast Nafion as at T = 120°C.

Moreover, the long term stability of fuel cell performance for magnetically aligned Nafion/CS-SPION nanocomposite membrane at 120 °C was measured at both RH of 40% and 100% over 150 h. As seen in Figure 5, the performance of designed nanocpmposites remains quite stable for a long time during continuous operation. The results confirm stable aligned ionic nanodomains inside Nafion matrix.

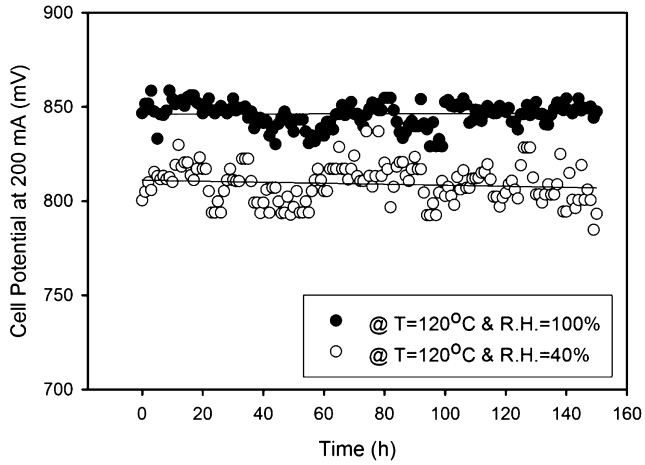

Figure 5. Long term stability of fuel cell performance characterized by measuring cell potential of MEAs based on magnetically aligned Nafion/CS-SPION nanocomposite membranes at 200 mA; The data were collected at 120°C at two different relative humidities of 40% and 100%.

4. CONCLUSION

These results clearly confirmed superior properties of aligned nanocomposite membranes over the entire parameter range of interest. Such an observation confirms the importance of unidirectional proton conduction on the overall performance of fuel cell systems. These types of membrane can be considered as high-performance proton exchange membranes for PEMFC applications.

AUTHOR INFORMATION

Corresponding Authors

*E-mail: mahdi.hasani@gmail.com.

*E-mail: geraldine.coullerez@epfl.ch.
*E-mail: karl.jacob@mse.gatech.edu. Tel.: +1 404 894 2541.
*E-mail: philippe.renaud@epfl.ch. Tel.: +41 21 693 67 97. Fax: +41 21 693 59 50.

Author Contributions

The manuscript was written through contributions of all authors. All authors have given approval to the final version of the manuscript.

Notes

The authors declare no competing financial interest.

■ ACKNOWLEDGMENTS

This research is performed in the framework of Biologically Inspired Developing Advanced Research (BiDAR) group.

■ REFERENCES

(1) Zhang, H.; Shen, P. K. Advances in the High Performance Polymer Electrolyte Membranes for Fuel Cells. *Chem. Soc. Rev.* **2012**, *41* (6), 2382−2394.
(2) Steele, B. C. H.; Heinzel, A. Materials for Fuel-Cell Technologies. *Nature* **2001**, *414* (6861), 345−352.
(3) Bose, S.; Kuila, T.; Nguyen, T. X. H.; Kim, N. H.; Lau, K.-t.; Lee, J. H. Polymer Membranes for High Temperature Proton Exchange Membrane Fuel Cell: Recent Advances and Challenges. *Prog. Polym. Sci.* **2011**, *36* (6), 813−843.
(4) Schmidt-Rohr, K.; Chen, Q. Parallel Cylindrical Water Nanochannels in Nafion Fuel-Cell Membranes. *Nat. Mater.* **2008**, *7* (1), 75−83.
(5) Diat, O.; Gebel, G. Fuel Cells: Proton Channels. *Nat. Mater.* **2008**, *7* (1), 13−14.
(6) Ma, C.-H.; Yu, T. L.; Lin, H.-L.; Huang, Y.-T.; Chen, Y.-L.; Jeng, U. S.; Lai, Y.-H.; Sun, Y.-S. Morphology and Properties of Nafion Membranes Prepared by Solution Casting. *Polymer* **2009**, *50* (7), 1764−1777.
(7) Dong, B.; Gwee, L.; Salas-de la Cruz, D.; Winey, K. I.; Elabd, Y. A. Super Proton Conductive High-Purity Nafion Nanofibers. *Nano Lett.* **2010**, *10* (9), 3785−3790.
(8) Tamura, T.; Kawakami, H. Aligned Electrospun Nanofiber Composite Membranes for Fuel Cell Electrolytes. *Nano Lett.* **2002**, *10* (4), 1324−1328.
(9) Hasani-Sadrabadi, M. M.; Shabani, I.; Soleimani, M.; Moaddel, H. Novel Nanofiber-Based Triple-Layer Proton Exchange Membranes for Fuel Cell Applications. *J. Power Sources* **2011**, *196* (10), 4599−4603.
(10) Li, J.; Park, J. K.; Moore, R. B.; Madsen, L. A. Linear Coupling of Alignment with Transport in a Polymer Electrolyte Membrane. *Nat. Mater.* **2011**, *10* (7), 507−511.
(11) Bureekaew, S.; Horike, S.; Higuchi, M.; Mizuno, M.; Kawamura, T.; Tanaka, D.; Yanai, N.; Kitagawa, S. One-Dimensional Imidazole Aggregate in Aluminium Porous Coordination Polymers with High Proton Conductivity. *Nat. Mater.* **2009**, *8* (10), 831−836.
(12) Yamaguchi, T.; Zhou, H.; Nakazawa, S.; Hara, N. An Extremely Low Methanol Crossover and Highly Durable Aromatic Pore-Filling Electrolyte Membrane for Direct Methanol Fuel Cells. *Adv. Mater.* **2007**, *19* (4), 592−596.
(13) Chen, H.; Palmese, G. R.; Elabd, Y. A. Membranes with Oriented Polyelectrolyte Nanodomains. *Chem. Mater.* **2006**, *18* (20), 4875−4881.
(14) Liu, D.; Yates, M. Z. Electric Field Processing to Control the Structure of Poly(Vinylidene Fluoride) Composite Proton Conducting Membranes. *J. Membr. Sci.* **2009**, *326* (2), 539−548.
(15) Liu, D.; Yates, M. Z. Tailoring the Structure of S-Peek/Pdms Proton Conductive Membranes through Applied Electric Fields. *J. Membr. Sci.* **2008**, *322* (1), 256−264.
(16) Gasa, J. V.; Boob, S.; Weiss, R. A.; Shaw, M. T. Proton-Exchange Membranes Composed of Slightly Sulfonated Poly(Ether Ketone Ketone) and Highly Sulfonated Crosslinked Polystyrene Particles. *J. Membr. Sci.* **2006**, *269* (1−2), 177−186.
(17) Oren, Y.; Freger, V.; Linder, C. Highly Conductive Ordered Heterogeneous Ion-Exchange Membranes. *J. Membr. Sci.* **2004**, *239* (1), 17−26.
(18) Ruotsalainen, T.; Torkkeli, M.; Serimaa, R.; Mäkelä, T.; Mäki-Ontto, R.; Ruokolainen, J.; ten Brinke, G.; Ikkala, O. Structural Hierarchy in Flow-Aligned Hexagonally Self-Organized Microphases with Parallel Polyelectrolytic Structures. *Macromolecules* **2003**, *36* (25), 9437−9442.
(19) Park, M. J.; Balsara, N. P. Anisotropic Proton Conduction in Aligned Block Copolymer Electrolyte Membranes at Equilibrium with Humid Air. *Macromolecules* **2009**, *43* (1), 292−298.
(20) Majewski, P. W.; Gopinadhan, M.; Osuji, C. O. Magnetic Field Alignment of Block Copolymers and Polymer Nanocomposites: Scalable Microstructure Control in Functional Soft Materials. *J. Polym. Sci. B: Polym. Phys.* **2012**, *50* (1), 2−8.
(21) Pelligra, C. I.; Majewski, P. W.; Osuji, C. O. Large Area Vertical Alignment of Zno Nanowires in Semiconducting Polymer Thin Films Directed by Magnetic Fields. *Nanoscale* **2013**, *5* (21), 10511−10517.
(22) Brijmohan, S. B.; Shaw, M. T. Magnetic Ion-Exchange Nanoparticles and Their Application in Proton Exchange Membranes. *J. Membr. Sci.* **2007**, *303* (1−2), 64−71.
(23) Hasanabadi, N.; Ghaffarian, S. R.; Hasani-Sadrabadi, M. M. Magnetic Field Aligned Nanocomposite Proton Exchange Membranes Based on Sulfonated Poly (Ether Sulfone) and Fe2O3 Nanoparticles for Direct Methanol Fuel Cell Application. *Int. J. Hydrogen Energy* **2011**, *36* (23), 15323−15332.
(24) Hasani-Sadrabadi, M. M.; Mokarram, N.; Azami, M.; Dashtimoghadam, E.; Majedi, F. S.; Jacob, K. I. Preparation and Characterization of Nanocomposite Polyelectrolyte Membranes Based on Nafion Ionomer and Nanocrystalline Hydroxyapatite. *Polymer* **2011**, *52* (5), 1286−1296.
(25) Hasani-Sadrabadi, M. M.; Dashtimoghadam, E.; Majedi, F. S.; Kabiri, K.; Mokarram, N.; Solati-Hashjin, M.; Moaddel, H. Novel High-Performance Nanohybrid Polyelectrolyte Membranes Based on Bio-Functionalized Montmorillonite for Fuel Cell Applications. *Chem. Commun.* **2010**, *46* (35), 6500−6502.
(26) Hasani-Sadrabadi, M. M.; Dashtimoghadam, E.; Majedi, F. S.; Kabiri, K. Nafion/Bio-Functionalized Montmorillonite Nanohybrids as Novel Polyelectrolyte Membranes for Direct Methanol Fuel Cells. *J. Power Sour* **2009**, *190* (2), 318−321.
(27) Petri-Fink, A.; Chastellain, M.; Juillerat-Jeanneret, L.; Ferrari, A.; Hofmann, H. Development of Functionalized Superparamagnetic Iron Oxide Nanoparticles for Interaction with Human Cancer Cells. *Biomaterials* **2005**, *26* (15), 2685−2694.
(28) Doan Thi Kim, D.; Tran Hoang, H.; Le Hong, P.; Bui Duc, L.; Le Khanh, V.; Phan Nha, T. Preparation and Characterization of Magnetic Nanoparticles with Chitosan Coating. *J. Phys: Conf Ser.* **2009**, *187* (1), 012036.
(29) Hasani-Sadrabadi, M. M.; Ghaffarian, S. R.; Mokarram-Dorri, N.; Dashtimoghadam, E.; Majedi, F. S. Characterization of Nanohybrid Membranes for Direct Methanol Fuel Cell Applications. *Solid State Ionics* **2009**, *180* (32-35), 1497−1504.
(30) Hasani-Sadrabadi, M. M.; Dashtimoghadam, E.; Sarikhani, K.; Majedi, F. S.; Khanbabaei, G. Electrochemical Investigation of Sulfonated Poly(Ether Ether Ketone)/Clay Nanocomposite Membranes for Moderate Temperature Fuel Cell Applications. *J. Power Sources* **2010**, *195* (9), 2450−2456.
(31) Li, L.; Shen, X.; Hong, S. W.; Hayward, R. C.; Russell, T. P. Fabrication of Co-Continuous Nanostructured and Porous Polymer Membranes: Spinodal Decomposition of Homopolymer and Random Copolymer Blends. *Angew. Chem., Int. Ed* **2012**, *51* (17), 4089−4094.
(32) Hasani-Sadrabadi, M. M.; Majedi, F. S.; VanDersarl, J. J.; Dashtimoghadam, E.; Ghaffarian, S. R.; Bertsch, A.; Moaddel, H.; Renaud, P. Morphological Tuning of Polymeric Nanoparticles via Microfluidic Platform for Fuel Cell Applications. *J. Am. Chem. Soc.* **2012**, *134* (46), 18904−18907.
(33) Lopez-Cruz, A.; Barrera, C.; Calero-DdelC, V. L.; Rinaldi, C. Water Dispersible Iron Oxide Nanoparticles Coated with Covalently Linked Chitosan. *J. Mater. Chem.* **2009**, *19* (37), 6870−6876.

(34) Majedi, F. S.; Hasani-Sadrabadi, M. M.; Emami, S. H.; Taghipoor, M.; Dashtimoghadam, E.; Bertsch, A.; Moaddel, H.; Renaud, P. Microfluidic Synthesis of Chitosan-Based Nanoparticles for Fuel Cell Applications. *Chem. Commun.* **2012**, *48* (62), 7744−7746.
(35) Chen, Y.; Thorn, M.; Christensen, S.; Versek, C.; Poe, A.; Hayward, R. C.; Tuominen, M. T. ThayumanavanS, Enhancement of Anhydrous Proton Transport by Supramolecular Nanochannels in Comb Polymers. *Nat. Chem.* **2010**, *2* (6), 503−508.
(36) Hasani-Sadrabadi, M. M.; Dashtimoghadam, E.; Mokarram, N.; Majedi, F. S.; Jacob, K. I. Triple-Layer Proton Exchange Membranes Based on Chitosan Biopolymer with Reduced Methanol Crossover for High-Performance Direct Methanol Fuel Cells Application. *Polymer* **2012**, *53* (13), 2643−2651.
(37) Choi, B. G.; Hong, J.; Park, Y. C.; Jung, D. H.; Hong, W. H.; Hammond, P. T.; Park, H. Innovative Polymer Nanocomposite Electrolytes: Nanoscale Manipulation of Ion Channels by Functionalized Graphenes. *ACS Nano* **2011**, *5* (6), 5167−5174.
(38) Yan, X.-M.; Mei, P.; Mi, Y.; Gao, L.; Qin, S. Proton Exchange Membrane with Hydrophilic Capillaries for Elevated Temperature Pem Fuel Cells. *Electrochem. Commun.* **2009**, *11* (1), 71−74.
(39) Majedi, F. S.; Hasani-Sadrabadi, M. M.; Dashtimoghadam, E.; Haghighi, A. H.; Bertsch, A.; Moaddel, H.; Renaud, P. Polybenzimidazole-Decorated Carbon Nanotube: A High-Performance Proton Conductor. *Phys. Status Solidi RRL* **2012**, *6* (7), 318−320.
(40) Adjemian, K. T.; Dominey, R.; Krishnan, L.; Ota, H.; Majsztrik, P.; Zhang, T.; Mann, J.; Kirby, B.; Gatto, L.; Velo-Simpson, M.; Leahy, J.; Srinivasan, S.; Benziger, J. B.; Bocarsly, A. B. Function and Characterization of Metal Oxide−Nafion Composite Membranes for Elevated-Temperature H_2/O_2 Pem Fuel Cells. *Chem. Mater.* **2006**, *18* (9), 2238−2248.
(41) Hasani-Sadrabadi, M. M.; Dashtimoghadam, E.; Nasseri, R.; Karkhaneh, A.; Majedi, F. S.; Mokarram, N.; Jacob, K. I. Cellulose Nanowhiskers to Regulate Microstructure of Perfluorosulfonate Ionomers for High-Performance Fuel Cell. *J. Mater. Chem. A* **2014**, DOI: 10.1039/c4ta00635f.